2013

β-Mn-Type Co8+xZn12−x as a Defect Cubic Laves Phase: Site Preferences, Magnetism, and Electronic Structure

Weiwei Xie
Iowa State University

Srinvasa Timmaiah
Iowa State University

Jagat Lamal
Iowa State University

Jing Liu
Iowa State University

Thomas W. Heitmann
University of Missouri
See next page for additional authors

β-Mn-Type Co8+xZn12−x as a Defect Cubic Laves Phase: Site Preferences, Magnetism, and Electronic Structure

Abstract

The results of crystallographic analysis, magnetic characterization, and theoretical assessment of β-Mn-type Co–Zn intermetallics prepared using high-temperature methods are presented. These β-Mn Co–Zn phases crystallize in the space group $P4_132$ [Pearson symbol $cP20$; $a = 6.3555(7)–6.3220(7)$], and their stoichiometry may be expressed as $Co_{8+x}Zn_{12-x}$ [$1.7(2) < x < 2.2(2)$]. According to a combination of single-crystal X-ray diffraction, neutron powder diffraction, and scanning electron microscopy, atomic site occupancies establish clear preferences for Co atoms in the 8c sites and Zn atoms in the 12d sites, with all additional Co atoms replacing some Zn atoms, a result that can be rationalized by electronic structure calculations. Magnetic measurements and neutron powder diffraction of an equimolar Co:Zn sample confirm ferromagnetism in this phase with a Curie temperature of ~420 K. Neutron powder diffraction and electronic structure calculations using the local spin density approximation indicate that the spontaneous magnetization of this phase arises exclusively from local moments at the Co atoms. Inspection of the atomic arrangements of $Co_{8+x}Zn_{12-x}$ reveals that the β-Mn aristotype may be derived from an ordered defect, cubic Laves phase ($MgCu_2$-type) structure. Structural optimization procedures using the Vienna ab initio simulation package (VASP) and starting from the undistorted, defect Laves phase structure achieved energy minimization at the observed β-Mn structure type, a result that offers greater insight into the β-Mn structure type and establishes a closer relationship with the corresponding α-Mn structure ($cI58$).

Disciplines

Biological and Chemical Physics | Materials Chemistry | Metallurgy | Physical Chemistry

Comments

Reprinted (adapted) with permission from *I*norg. Chem., 2013, 52 (16), pp 9399–9408. Copyright 2013 American Chemical Society.

Authors

Weiwei Xie, Srinvasa Timmaiah, Jagat Lamal, Jing Liu, Thomas W. Heitmann, Dante Quirinale, A. I. Goldman, Vitalij K. Pecharsky, and Gordon J. Miller

Inorganic Chemistry

Article

pubs.acs.org/IC

β-Mn-Type $Co_{8+x}Zn_{12-x}$ as a Defect Cubic Laves Phase: Site Preferences, Magnetism, and Electronic Structure

Weiwei Xie,[†] Srinivasa Thimmaiah,[†] Jagat Lamsal,[‡] Jing Liu,[§] Thomas W. Heitmann,[⊥] Dante Quirinale,[‡] Alan I. Goldman,[‡] Vitalij Pecharsky,[§] and Gordon J. Miller*[,†]

[†]Department of Chemistry, [‡]Department of Physics and Astronomy, and [§]Department of Material Science and Engineering, Iowa State University and Ames Laboratory, U.S. Department of Energy, Ames, Iowa 50011, United States

[⊥]The Missouri Research Reactor, University of Missouri, Columbia, Missouri 65211, United States

Supporting Information

ABSTRACT: The results of crystallographic analysis, magnetic characterization, and theoretical assessment of β-Mn-type Co−Zn intermetallics prepared using high-temperature methods are presented. These β-Mn Co−Zn phases crystallize in the space group $P4_132$ [Pearson symbol $cP20$; a = 6.3555(7)−6.3220(7)], and their stoichiometry may be expressed as $Co_{8+x}Zn_{12-x}$ [$1.7(2) < x < 2.2(2)$]. According to a combination of single-crystal X-ray diffraction, neutron powder diffraction, and scanning electron microscopy, atomic site occupancies establish clear preferences for Co atoms in the 8c sites and Zn atoms in the 12d sites, with all additional Co atoms replacing some Zn atoms, a result that can be rationalized by electronic structure calculations. Magnetic measurements and neutron powder diffraction of an equimolar Co:Zn sample confirm ferromagnetism in this phase with a Curie temperature of ∼420 K. Neutron powder diffraction and electronic structure calculations using the local spin density approximation indicate that the spontaneous magnetization of this phase arises exclusively from local moments at the Co atoms. Inspection of the atomic arrangements of $Co_{8+x}Zn_{12-x}$ reveals that the β-Mn aristotype may be derived from an ordered defect, cubic Laves phase ($MgCu_2$-type) structure. Structural optimization procedures using the Vienna ab initio simulation package (VASP) and starting from the undistorted, defect Laves phase structure achieved energy minimization at the observed β-Mn structure type, a result that offers greater insight into the β-Mn structure type and establishes a closer relationship with the corresponding α-Mn structure ($cI58$).

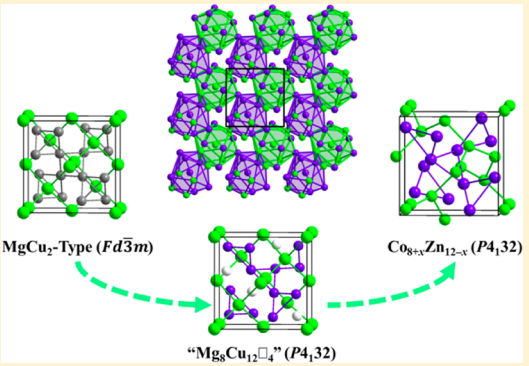

INTRODUCTION

Understanding the relationships among the structure, composition, bonding, and properties of complex intermetallic compounds remains both fascinating and challenging because few general predictive strategies have emerged that allow targeted synthesis of novel compounds with specific properties. For compounds involving the late- and post-transition metals, the Hume-Rothery electron-counting rules,[1] which emphasize the valence s and p electrons in the compound, can be used to rationalize the crystal structure. However, if a system exhibits partially filled d bands, then these rules to predict crystal structures typically incorporate negative valences for the transition metals but cannot rationalize some subtle structural distortions or element distributions.[2] Electronic structure calculations have successfully identified some patterns of band structure and occupancies in γ-brass Fe−Zn,[3] Ni−Zn,[3] and M−Ga (M = Cr−Fe)[4−6] cases, yet no reports have examined the noncentrosymmetric cubic β-Mn-type systems in any systematic way. For example, unlike Fe or Ni, which reacts with Zn in a 1:1 molar ratio to form a β-brass, Co is reported to form a β-Mn-type structure with Zn.[7−9] However, other than a lattice constant, no other structural details have been reported.[10] Therefore, investigating the Co−Zn system may help us to understand how 3d transition metals control the crystal structures within the framework of the Hume-Rothery rules.

The Co−Zn system shows some anomalies in its phase equilibria arising, in part, from the magnetic transition associated with Co.[8] Ferromagnetism in elemental Co certainly influences its anomalous ground-state structure, which is hexagonally close-packed and not cubic close-packed like Rh and Ir, by breaking the degeneracy between spin-up and spin-down electronic states. Ferromagnetic "$Co_{0.5}Zn_{0.5}$", which is the Co-richest intermetallic in the Co−Zn system and has been assigned the cubic β-Mn type (Strukturbericht designation $A13$), was explored for its magnetooptical properties several decades ago.[10] In recent years, the Zn-rich region of the Co−Zn diagram has been reinvestigated for two brasslike structures, δ-Co_2Zn_{15} and δ_1-$CoZn_{7.8}$,[11,12] the first of which shows an interesting double helix of icosahedra. However, there are only a few reports of Co-rich Co−Zn phases,[8,10] and even any characterization of β-Mn-type Co−Zn phases remains limited other than a lattice constant (a = 6.319 Å), its room temperature magnetization (39 A·m^2/kg), and the polar Kerr

Received: April 19, 2013
Published: August 2, 2013

   dx.doi.org/10.1021/ic4009653 | Inorg. Chem. 2013, 52, 9399−9408

Table 1. Compositions, Phase Analyses, Lattice Constants, And Refined Compositions for β-Mn-Type $Co_{8+\delta}Zn_{12-\delta}$ Phases (PXRD = Powder X-ray Diffraction; SCXRD = Single-Crystal X-ray Diffraction)

		a (Å)			composition		
atom % Zn loaded	phases (PXRD)	PXRD[a]	SCXRD[a]	NPD	SCXRD	SEM	NPD
35.04(1)	β-Mn, hcp-Co	6.315(5)					
40.33(1)	β-Mn, hcp-Co	6.319(2)	6.322(1)		$Co_{10.2(4)}Zn_{9.8}$	$Co_{10.1(2)}Zn_{9.9(2)}$	
45.06(1)	β-Mn, hcp-Co	6.327(4)					
49.85(1)	β-Mn	6.329(7)	6.337(6)	6.3342(1)[b] 6.3547(2)[c]	$Co_{10.0(4)}Zn_{10.0}$	$Co_{9.8(2)}Zn_{10.2(2)}$	$Co_{10.4(2)}Zn_{9.6(2)}$
55.01(1)	β-Mn	6.331(6)					
60.03(1)	β-Mn, γ-brass	6.339(7)	6.341(2)		$Co_{9.9(4)}Zn_{10.1}$	$Co_{9.5(2)}Zn_{10.5(2)}$	
65.10(1)	β-Mn, γ-brass	6.344(7)	6.356(3)		$Co_{9.7(2)}Zn_{10.3}$		

[a]293 K; numbers in parentheses are standard uncertainties using at least two different measurements of similar loadings. [b]293 K; numbers in parentheses are standard uncertainties in the last given digit from standard deviation of Rietveld fits. [c]500 K; numbers in parentheses are standard uncertainties in the last given digit from standard deviation of Rietveld fits.

rotation angle (−0.25° at 633 and 830 nm).[10] The recent observation of skyrmions, which are described as vortex-like spin structures, in noncentrosymmetric cubic magnetic solids like MnSi and FeGe provides additional impetus for a closer examination of the noncentrosymmetric β-Mn-type systems that contain magnetically active metals.[13−15] In particular, nuclear quadrupole resonance studies[16] on β-Mn itself show that inequivalent Mn atoms contribute differently to its overall magnetism. Moreover, there is a close structural relationship between octagonal quasicrystals and the β-Mn structure.[17−20]

With these magnetic and structural features in mind, we report herein a thorough structural characterization and investigation of the magnetic properties and theoretical electronic structures of β-Mn-type Co−Zn phases, with an emphasis on the elemental distribution throughout the unit cell, local magnetic moments, and chemical bonding. In a subsequent study, we will examine the electronic states and bonding features with respect to other related intermetallic phases.

EXPERIMENTAL SECTION

Synthesis. β-Mn-type Co−Zn phases were obtained by the fusion of mixtures of Co pieces (99.9%, Ames Laboratory) and Zn particles (99.99%, Alfa Aesar), combinations that ranged from 35 to 65 mol % Zn. Each reactant mixture, about 500 mg total, was sealed into an evacuated silica tube ($<10^{-5}$ Torr), heated to 1000 °C for 12 h, followed by cooling to 925 °C at a rate of 1 °C/h, and annealed at this temperature for 3 days, after which the container was quenched into water or slowly cooled in the furnace. Seven different Co−Zn samples were prepared (see Table 1). Of these, the three Zn-rich loadings yielded a mixture of β-Mn-type and γ-brass Co_2Zn_{11}. The two Co-rich samples contained β-Mn-type compounds and Co particles. Only the two intermediate loadings, i.e., 50 and 55 mol % Zn, led to single-phase β-Mn-type compounds. Using an optical microscope, the β-Mn-type crystals adopt tetragonal block shapes, whereas γ-brass Co_2Zn_{11} crystals have elongated rectangular morphologies. All products are stable toward decomposition in air and moisture but react with dilute acid at room temperature.

Phase Analyses. All samples were finely ground and examined by powder X-ray diffraction for identification and phase purity on a STOE WinXPOW powder diffractometer employing Cu radiation ($\lambda_{K\alpha}$= 1.5406 Å) for all of the samples. The scattered intensity was recorded as a function of the Bragg angle (2θ) using a scintillation detector with a step of 0.03° 2θ in step scan mode, ranging from 0° to 130°. Phase identification was accomplished using the program *PowderCell*,[21] and lattice parameters from manually selected β-Mn-type crystals were refined by Bragg's law using a silicon 640*b* powder X-ray diffraction position standard (NIST; a = 5.430940 ± 0.000035 Å).

Because X-ray fluorescence can create a high background for Co-containing samples examined using Cu Kα radiation, the powder X-ray diffraction patterns of three samples showing high yields of a β-Mn phase, i.e., those loaded with 40, 50, and 60 atom % Zn, were also collected on a Philips PANalytical X'pert-Pro powder diffractometer using Co radiation ($\lambda_{K\alpha}$ =1.7903 Å). The scattered intensities were recorded in step scan mode with 0.008° steps over a 2θ range from 5° to 100°. For these measurements, phase identification and the lattice parameters were refined by full-profile Rietveld[22] refinements using *LHPM RIETICA*.[23]

Structure Determination. Crystals from each reaction sample were mounted on the tips of glass fibers. Room temperature intensity data were collected on a Bruker SMART Apex CCD diffractometer using Mo Kα radiation (λ = 0.71073 Å). Data were collected over a full sphere of reciprocal space by taking three sets of 606 frames with 0.3° scans in ω with an exposure time of 10 s per frame. The 2θ range extended from 8° to 60°. The *SMART* software was used for data acquisition. Intensities were extracted and corrected for Lorentz and polarization effects using the *SAINT* program. Empirical absorption corrections were accomplished with *SADABS*, which is based on modeling transmission by spherical harmonics employing equivalent reflections with $I > 3\sigma(I)$.[24,25] With the *SHELXTL* package,[26] the crystal structures were solved using direct methods and refined by full-matrix least squares on F^2. All crystal structure drawings were produced using the program *Diamond*.[27]

Neutron Powder Diffraction (NPD). NPD measurements on a polycrystalline sample with a nominal composition of $Co_{50.15(1)}Zn_{49.85(1)}$, which produced the highest yield of β-Mn-type compound, were performed on the high-resolution powder diffractometer at the University of Missouri Research Reactor using a double-focusing Si (511) crystal monochromator to select neutrons with a wavelength λ = 1.4803 Å. To obtain sufficient samples for NPD measurements, ~1.3 g of polycrystalline $Co_{50.01(1)}Zn_{49.99(1)}$ was loaded into a V sample holder (7.5 cm length and 3.0 mm diameter). A set of five linear position-sensitive detectors were employed to collect a series of 19° sections of the diffraction pattern; the full diffraction pattern was measured in five steps to a $2\theta_{max}$ value of 108°. This powder diffractometer uses a radial oscillating collimator that averages the shadow of the collimator blades at every channel. The large detector areas allow very weak magnetic peaks to be detected by neutrons with high statistical accuracy. The NPD pattern at 293 K was taken in air, whereas the pattern at 500 K was collected using a high-temperature furnace. We note that the large amount of material contained with the high-temperature furnace results in a high background in the low-angle segment of the patterns. Therefore, the empty furnace background was subtracted from the powder diffraction pattern collected for the sample in the high-temperature furnace to represent the diffraction pattern from the sample only. Analysis of the NPD data was performed by the Rietveld method using the program *FULLPROF*.[28]

Scanning Electron Microscopy (SEM). Characterization was completed using variable-pressure SEM (Hitachi S-2460N) and energy-dispersive spectroscopy (EDS; Oxford Instruments Isis X-ray analyzer). Samples were mounted in epoxy, carefully polished, and

dx.doi.org/10.1021/ic4009653 | Inorg. Chem. 2013, 52, 9399−9408

Table 2. Single-Crystal Crystallographic Data for β-Mn-Type Co−Zn Phases at 293(2) K

loaded compd (atom % Zn)	40.33(1)	49.85(1)	60.03(1)	65.10(1)
refined formula	$Co_{10.2(2)}Zn_{9.8}$	$Co_{10.0(2)}Zn_{10.0}$	$Co_{9.8(2)}Zn_{10.2}$	$Co_{9.7(2)}Zn_{10.3}$
fw (g/mol)	1241.39	1242.94	1244.48	1244.88
$F(000)$	1138	1140	1142	1142
a (Å)	6.3220(7)	6.3358(14)	6.3450(7)	6.3555(7)
V (Å^3)	252.68(5)	254.33(10)	255.44(5)	256.71(5)
d_{calc} (Mg/m^3)	8.158	8.115	8.093	8.041
abs corr	empirical	empirical	empirical	empirical
ext coeff	0.018(2)	0.004(1)	0.014(4)	0.003(1)
μ (mm^{-1})	38.879	38.800	38.856	38.656
θ_{range} (deg)	4.56−28.05	4.55−27.99	4.54−27.94	4.54−28.32
hkl ranges	$-8 \le h, k, l \le 8$	$-8 \le h, k, l \le 8$	$-8 \le h, k, l \le 8$	$-8 \le h, k, l \le 8$
no. of reflns (R_{int})	1572 (0.0467)	1570 (0.0376)	2216 (0.0287)	2205 (0.0245)
no. of indep reflns	110	109	110	111
no. of param	12	12	12	12
R1, wR2 (all I)	0.0170, 0.337	0.0167, 0.0280	0.0115, 0.0278	0.0146, 0.0290
GOF	1.285	1.180	1.358	1.321
peak, hole (e/Å^3)	0.432, −0.463	0.320, −0.353	0.407, −0.388	0.405, −0.442

then sputter-coated with a thin layer of carbon prior to loading into the SEM chamber. The samples were examined at 20 kV. Spectra were collected for 100 s. An Oxford Instruments Tetra backscattered electron (BSE) detector was used to image the samples using the BSE signal. Multiple points were examined in each phase within multiple grains of a specimen. Compositional estimates were calculated using Oxford's SEM *Quant* software to correct intensities for matrix effects.

Magnetization Measurements. The magnetization measurements were performed using a superconducting quantum interference device (SQUID) magnetometer MPMS XL-7 and Vibrating Sample Magnetometer (VSM) EV11 manufactured by Quantum Design, Inc., on pieces of β-Mn-type single crystals that were manually selected from the product obtained from the loading with 49.85(1) atom % Zn. The SQUID operates over a temperature range of 2−300 K and in applied fields of up to 70 kOe. The samples were placed in glass capsules for measurement. The VSM was operated from 300 to 900 K.

NPD at 293 K also gives a magnetic contribution to nuclear Bragg reflections, which facilitates refinement of the magnetic moments on each atom.

Electronic Structure Calculations. *Tight-Binding, Linear Muffin Tin Orbital Atomic Spheres Approximation (TB-LMTO-ASA).*[29] Calculations of the electronic and possible magnetic structures were performed by TB-LMTO-ASA using the Stuttgart code. Exchange and correlation were treated by the local density approximation (LDA) and the local spin-density approximation (LSDA).[30] In the ASA method, space is filled with overlapping Wigner−Seitz (WS) spheres. The symmetry of the potential is considered spherical inside each WS sphere, and a combined correction is used to take into account the overlapping part. The WS radii are 1.34 Å for Co and 1.52 Å for Zn. No empty spheres are necessary, and the overlap of WS spheres is limited to no larger than 16%. The basis set for the calculations included Co 4s, 4p, and 3d and Zn 4s, 4p, and 3d wave functions.[31] The convergence criterion was set to 0.1 meV. A mesh of 60 k points in the irreducible wedge of the first Brillouin zone was used to obtain all integrated values, including the density of states (DOS) and crystal orbital Hamiltonian population (COHP) curves.

Vienna ab Initio Simulation Package[32−35] *(VASP).* Structure optimization and charge-density calculations[36−38] were completed using VASP, which employs projector-augmented-wave pseudopotentials that were adopted with the Perdew−Burke−Ernzerhof generalized gradient approximation (PBE-GGA), in which scalar relativistic effects are included. For structural optimization, the conjugate gradient algorithm was applied. The energy cutoff was 346.1 eV. Reciprocal space integrations were completed over a 9 × 9 × 9 Monkhorst−Pack k-point mesh[39] with the linear tetrahedron method.[40] With these settings, the calculated total energy converged to less than 0.1 meV per atom.

RESULTS AND DISCUSSION

According to the Co−Zn phase diagram,[8] β-Mn-type phases exist between ∼49 and 58 atom % Zn, but this range narrows significantly to ∼50 atom % Zn above ∼920 °C. Although the phase diagram indicates the existence of a "high-temperature ZnCo" phase, which may adopt the β-brass[7] (*cP*2- or *cI*2-type) structure in the range 820−870 °C, our synthetic approach did not yield anything other than crystalline β-Mn-type product. Because this structure type involves two sites with different multiplicities, i.e., 8c and 12d, elucidation of the Co/Zn distribution is warranted. This aspect of the structural chemistry may also influence the bulk magnetic properties. In the course of investigating this Co−Zn phase, we identified an exceptional relationship between the structure of β-Mn and an extremely common intermetallic structure, the cubic Laves phase $MgCu_2$ type.

Phase Analyses. In accordance with the reported Co−Zn phase diagram, synthetic attempts to prepare β-Mn-type Co−Zn phases yielded mixtures of phases for Co- or Zn-rich loadings. Only those reactant mixtures that were loaded approximately 50 and 55 atom % Zn yielded single-phase crystalline products. Co-rich loadings produced hcp-Co particles, which could contain significant fractions of Zn as a substitutional solid solution. On the other hand, Zn-rich reactions yielded a γ-brass Co−Zn phase in addition to a β-Mn-type product. Table 1 summarizes the synthetic results; the powder X-ray diffraction patterns and electron micrographs of selected samples are illustrated in Figures S1 and S2 in the Supporting Information.

For the powder X-ray diffraction patterns, all scale factors and lattice parameters were refined, whereas the displacement parameters of all atoms were assumed to be isotropic at $B = 0.6$ according to NPD measurement and were not refined. The resulting profile residuals R_p varied between ca. 1.6 and 2.8 with weighted profile residuals R_{wp} between ca. 2.2 and 4.0. The refined lattice parameters for β-Mn-type Co−Zn phases showed a 0.46(8)% increase according to powder X-ray diffraction as the Zn loading increased from 35 to 65 atom %. Single crystals extracted from four reaction products showed a similar trend, +0.54(6)%. Analyses of the samples, whether by refinements from single-crystal diffraction or NPD or by SEM, all fall within 2 standard deviations of an equimolar ratio of

dx.doi.org/10.1021/ic4009653 | Inorg. Chem. 2013, 52, 9399−9408

Table 3. Atomic Coordinates, Site Occupancies, and Equivalent Isotropic Displacement Parameters of β-Mn-Type Co−Zn Phases at 293(2) K[a]

atom	Wyckoff site	occupancy	x	y	z	U_{eq}
			$Co_{10.2(2)}Zn_{9.8}$			
Zn/Co	12d	0.81(3)/0.19	$^1/_8$	0.2031(1)	0.4531(1)	0.0100(3)
Co	8c	1	0.0649(1)	0.0649(1)	0.0649(1)	0.0072(3)
			$Co_{10.0(2)}Zn_{10.0}$			
Zn/Co	12d	0.83(3)/0.17	$^1/_8$	0.2030(1)	0.4530(1)	0.0108(3)
Co	8c	1	0.0648(1)	0.0648(1)	0.0648(1)	0.0081(3)
			$Co_{9.8(2)}Zn_{10.2}$			
Zn/Co	12d	0.86(2)/0.14	$^1/_8$	0.2030(1)	0.4530(1)	0.0099(2)
Co	8c	1	0.0648(1)	0.0648(1)	0.0648(1)	0.0073(2)
			$Co_{9.7(2)}Zn_{10.3}$			
Zn/Co	12d	0.86(2)/0.14	$^1/_8$	0.2028(1)	0.4528(1)	0.0095(2)
Co	8c	1	0.0648(1)	0.0648(1)	0.0648(1)	0.0075(3)

[a] U_{eq} is defined as one-third of the trace of the orthogonalized U_{ij} tensor (Å^2).

Co:Zn in this phase. Therefore, β-Mn-type Co−Zn phases exhibit a small homogeneity region centered at 50 mol % Zn when quenched from 925 °C. From our powder diffraction results, the lower bound for the Zn content lies between 40 and 45 atom %, whereas the upper bound is 55−60 atom %. The results from single-crystal diffraction suggest an even narrower range (see the discussion below).

Because the published phase diagrams[7,8,41] from the last 25 years show various homogeneity widths of this Co−Zn phase region toward lower temperatures, three samples loaded with 40, 50, and 60 atom % Zn were heated to 1000 °C at a rate of 1 °C/min, kept for 12 h, and then cooled to 600 °C at 1 °C/min, at which point they were annealed for 3 weeks. Upon cooling to room temperature, powder X-ray diffraction patterns showed β-Mn-type Co−Zn phases in all three, with increasing lattice constants [6.3526(1), 6.3570(1), and 6.3601(1) Å] with increasing loaded Zn content. Moreover, the Zn-richest sample also contained γ-brass-type phase, the Co-richest sample indicated hcp-Co, and the 50:50 sample was essentially single phase. These results confirm that the β-Mn-type Co−Zn phase exists over a broad range of concentrations as the temperature is lowered to 600 °C.

Structure Determination and Site Preferences. To obtain further insight into the structural features of these β-Mn-type Co−Zn phases, single crystals were investigated to extract elemental distributions and an accurate determination of interatomic distances and coordination environments. The results of single-crystal diffraction on specimens extracted from four distinct loadings are summarized in Tables 2 and 3. Corresponding anisotropic displacement parameters and significant interatomic distances are summarized in Tables S1 and S2 in the Supporting Information. All structures crystallize in the noncentrosymmetric cubic space group $P4_132$ (No. 213) with atoms located at the 8c (C_3 symmetry) and 12d (C_2 symmetry) sites. Regardless of refined compositions, the 8c sites are fully occupied by Co atoms, whereas the 12d sites accommodate a mixture of Co and Zn atoms. Therefore, a formulation of these phases is $Co_{8+x}Zn_{12-x}$, in which x ranges from ~1.7(2) to 2.2(2), to reflect this pattern of site occupation. Before embarking on a discussion of the structural subtleties of this Co−Zn phase, however, we have identified an interesting relationship between the complex β-Mn-type structure and that of the cubic Laves phase, $MgCu_2$ type.

β-Mn as an Ordered Defect Cubic Laves Phase. In a tantalizing description of the analogies between the structures of β-Mn and the molecular solid P_4S_3, as well as between those of α-Mn and white phosphorus, Nesper intimated possible relationships between the structures of α-Mn and β-Mn and tetrahedral structures.[42] As it turns out, the structure of β-Mn-type $Co_{8+x}Zn_{12-x}$ (space group $P4_132$; Pearson symbol $cP20$) can be derived from the cubic Laves phase $MgCu_2$ (space group $Fd\bar{3}m$; Pearson symbol $cF24$), both of which exhibit some close relationships with the diamond structure. In particular, the Mg atom sites (Wyckoff designation 8a) in the cubic Laves phase $MgCu_2$ form precisely a three-dimensional (3D) diamond network. Within the voids, Cu atoms (Wyckoff designation 16d) form a 3D framework of vertex-sharing tetrahedra, as emphasized in Figure 1. The formulation of the complete cubic unit cell of this cubic Laves phase is, therefore, Mg_8Cu_{16}. After transformation of the unit cell of the Laves phase from (a, b, c) to (−b, a, c) and the orderly removal of four atoms from the 16d(Cu) sites, one from each tetrahedron located around the (revised) coordinates ($^1/_4$, $^1/_4$, $^1/_4$), ($^3/_4$, $^3/_4$, $^1/_4$), ($^1/_4$, $^3/_4$, $^3/_4$), and ($^3/_4$, $^1/_4$, $^3/_4$), a cubic "Mg_8Cu_{12}" unit cell can be created with space group $P4_132$ (see also Figure 1). Here, the

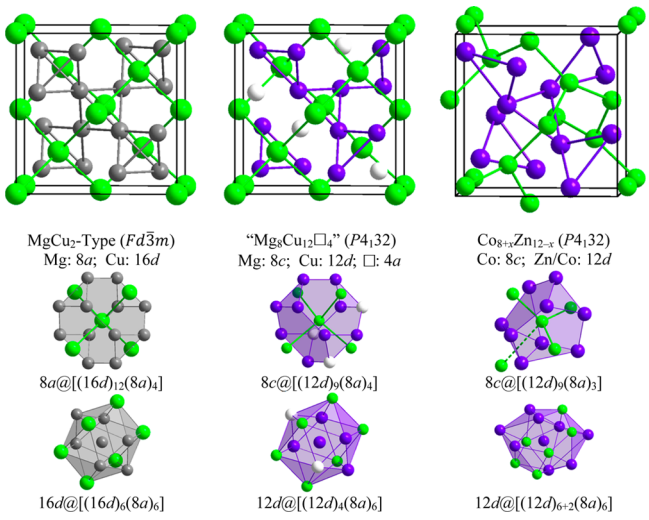

Figure 1. Unit cell and atomic coordination environments showing the relationship between the $MgCu_2$-type, cubic Laves phase structure and the β-Mn-type $Co_{8+x}Zn_{12-x}$: (left) $MgCu_2$ type (Mg, green; Cu, gray); (middle) hypothetical $Mg_8Cu_{12}\square_4$ (Mg, green; Cu, purple; □, white); (right) β-Mn-type $Co_{8+x}Zn_{12-x}$ (Co, green; Zn/Co, purple).

dx.doi.org/10.1021/ic4009653 | Inorg. Chem. 2013, 52, 9399−9408

Mg and Cu sites become respectively 8c and 12d, and the 4-fold vacant positions are 4a in the noncentrosymmetric space group. Relaxation of this hypothetical ordered defect cubic Laves phase structure yields the β-Mn structure type for $Co_{8+x}Zn_{12-x}$. We note that the vacant 4a sites are occupied by C atoms in Mo_3Al_2C[45] or N atoms in Mo_3Ni_2N.[43]

To study further this relationship between the cubic Laves phase ($cF24$) and β-Mn ($cP20$) structure types, a series of hypothetical "Co_8Zn_{12}" structures was constructed starting with "Co_8Zn_{16}" in space group $Fd\bar{3}m$ and following the algorithm discussed in the previous paragraph. The question becomes, how many distinct ways can one atomic site be removed from each of the four tetrahedra formed by the 16d sites? Because there are four tetrahedra, each with four atomic sites, it might appear that there are $4^4 = 256$ different possibilities. However, rotations, reflections, and translations will cause many of these options to be equivalent. This counting problem can be solved by using Burnside's lemma,[44] which allows enumeration of distinct isomers ("orbits") in a set of structures that is permuted by a group. For this problem, it turns out that there are nine distinct solutions, labeled α–ι,[44] which are listed and illustrated in Figure S3 in the Supporting Information. For each ordered vacancy structure, "Co_8Zn_{12}", a complete structural optimization was carried out using VASP. Table 4 lists the total energies per atom relative to the lowest-energy case before and after the structural relaxation. The arrangement of vacancies that gives the lowest energy before relaxation is model η, the one most closely related to the β-Mn-type structure, space group $P4_132$. Upon relaxation, the atoms at the 8c sites shift from (0, 0, 0) along body diagonals to final coordinates (x, x, x; $x = 0.0649$), whereas the atoms at the 12d sites shift from ($^1/_8$, $^1/_8$, $^3/_8$) along face diagonals to final coordinates ($^1/_8$, y, $y + {}^1/_4$; $y = 0.2029$). A comparison with the crystallographic results in Table 3 indicates excellent agreement between the calculated ground state of the ordered defect structure and the experimentally determined parameters of β-Mn-type $Co_{8+x}Zn_{12-x}$.

Table 4. Pearson Symbols, Volume (Å^3/atom) after Relaxation, Relative Total Energies (eV/atom) before and after Relaxation, and Relative Electrostatic ("metallic") Energies (eV/atom) before Relaxation for the Nine Ordered Defect Models of "Co_8Zn_{12}"[a]

model	Pearson symbol	volume/atom (Å^3)	ΔE_{TOT}/atom(before) (eV)	ΔE_{TOT}/atom(after) (eV)	ΔE_{ES}/atom(before) (eV)
α	$hR15$	12.20	0.4504	0.2292	39.7767
β	$mS40$	11.59	0.2255	0.2118	15.2145
γ	$oP10$	12.64	0.2130	0.1919	19.4932
δ	$mS20$	12.01	0.3631	0.4215	13.4378
ε	$aP20$	11.71	0.4180	0.1131	56.3823
θ	$cI40$	13.21	0.2349	0.2682	61.3661
η	$cP20$	11.51	0	0	0
ζ	$mS40$	12.43	0.1827	0.1301	17.5775
ι	$tP20$	12.27	0.1809	0.2374	15.7561

[a]The labels of the models follow the assignment of an analogous problem in ref 45.

Assessment of the total energies after relaxation reveals that a major driving force for the ordering of defects comes from the electrostatic energy between the conduction electrons and the arrangement of atomic cores,[46] which gives its lowest value for model η (the β-Mn arrangement). This effect also leads to the lowest atomic volume for model η. Further analysis suggests that two-center orbital interactions prefer the alternative models ε and θ, both of which show the two highest electrostatic energies. Because these energy values can be dependent on the valence electron count, i.e., energy band filling, we are examining the variation in the defect ordering as a function of the electron count, and other structural alternatives to the β-Mn structure type in the Co–Zn and related systems, and will report these results in a forthcoming paper.

Site Preferences in β-Mn-Type Co–Zn Phases. An expanded view of the unit cell and coordination polyhedra for β-Mn-type $Co_{8+x}Zn_{12-x}$ is shown in Figure 2. The polyhedral environments for each site in $Co_{8+x}Zn_{12-x}$ are Frank–Kasper polyhedra. The 8c(Co) site is surrounded by a distorted icosahedron consisting of three other 8c(Co) sites and nine 12d(Zn/Co) sites. On the other hand, each 12d(Zn/Co) site is coordinated by a 14-vertex polyhedron of six 8c(Co) and eight 12d(Zn/Co). Thus, given the refined site occupancies for the 12d sites, each 8c Co atom is coordinated, on average, by 4.2(2)–4.7(2) Co atoms and 7.8–7.2 Zn atoms, whereas each 12d site is surrounded by 7.0(2)–7.5(2) Co atoms and 7.0–6.5 Zn atoms. Such Frank–Kasper polyhedra are signature building blocks of tetrahedrally close-packed (tcp) solids, which are common among transition-metal intermetallics.[47,48] Examples of tcp solids include the cubic $MgCu_2$-type and hexagonal $MgZn_2$-type Laves phases as well as the structure of α-Mn, which is also called the χ phase. These structures, which are influenced by their valence electron concentrations or valence electron-to-atom ratios,[49] are composed of densely packed tetrahedra. The β-Mn type may also be assigned among the tcp solids because each unit cell contains four distinct $[(8c)_2(12d)_3]$ trigonal bipyramids (two face-sharing tetrahedra) that are linked to each other via additional tetrahedra. In the series of $Co_{8+x}Zn_{12-x}$ crystals, the shortest distances occur between neighboring 8c(Co) sites; these are ~2.37 Å, which are ~5% shorter than the nearest-neighbor Co–Co distances in hcp-Co (~2.50 Å). The 8c–12d(Co–Zn/Co) interatomic distances range from 2.59 to 2.70 Å, whereas the 12d–12d(Zn/Co–Zn/Co) distances are more uniform, viz., 2.65–2.68 Å. Both of these distance ranges are in line with the six shorter Zn–Zn distances (~2.66 Å) in hcp-Zn. Moreover, these structural features of the $Co_{8+x}Zn_{12-x}$ series are similar to the distance relationships in β-Mn (Mn_{20}), itself, and Re_3Fe_2.[43,50–52] Other related phases, e.g., Mg_3Ru_2[50] and Mo_3Ni_2N,[43] have somewhat different distance relationships (see Table S3 in the Supporting Information), which is part of the detailed structural/computational investigation that is currently underway for these complex intermetallics.

Because Co and Zn differ by only approximately 10% in X-ray scattering functions, a sample loaded with an equimolar mixture of Co and Zn was prepared for NPD experiments as described above. The neutron scattering lengths for Co (2.49 fm) and Zn (5.68 fm) differ significantly. However, because neutron diffraction is also sensitive to magnetic ordering, data were taken both above and below the Curie point, i.e., ~420 K (see Figure 3 and the subsequent section on magnetic characterization), yielded structural parameters that concur with the results of single-crystal X-ray diffraction; these results are summarized in Table 5. Again, the 8c site refined to be fully occupied by Co. Refinement of the 12d site yielded ~80% Zn for an overall composition that is slightly Co-rich, i.e., $Co_{10.4(2)}Zn_{9.6}$. Furthermore, as part of this refinement, the 12d site was constrained to be fully occupied by a mixture of

dx.doi.org/10.1021/ic4009653 | Inorg. Chem. 2013, 52, 9399–9408

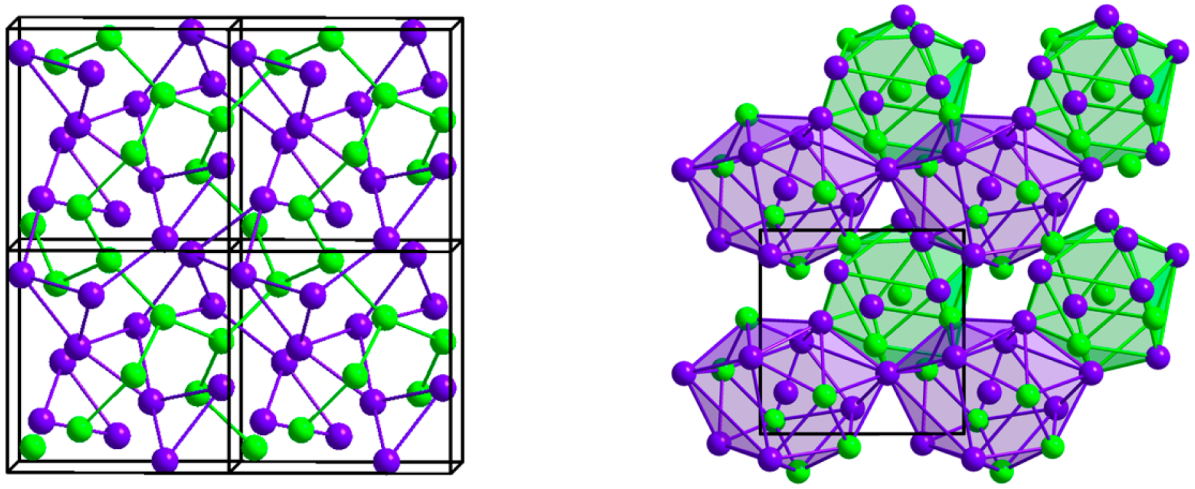

Figure 2. Crystal structure of β-Mn-type $Co_{8+x}Zn_{12-x}$ showing (left) four unit cells with the 8c−8c and 12d−12d connections emphasized and (right) a (001) view emphasizing the coordination polyhedra surrounding the 8c (green) and 12d (purple) sites.

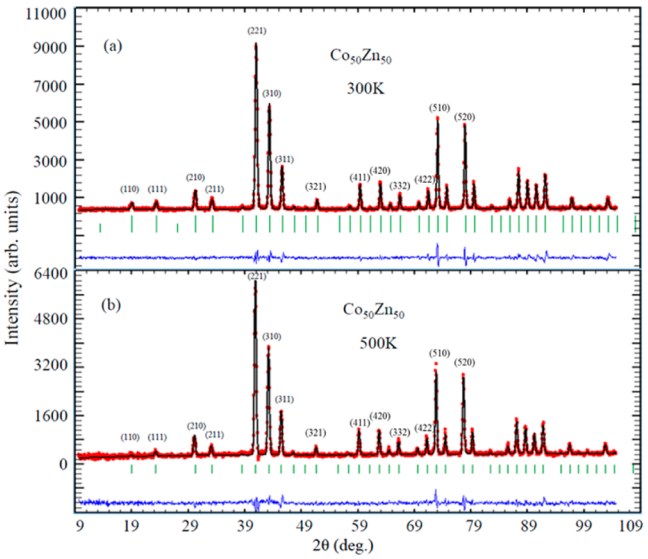

Figure 3. Neutron diffraction profile fits from the Rietveld method using *FULLPROF* for $Co_{50}Zn_{50}$: (a) nuclear and magnetic Bragg reflections at 293 K; (b) nuclear Bragg reflections at 500 K. The observed data points are given by red circles, the calculated intensity pattern is given by black solid lines, and the corresponding residual (i.e., the difference between the observed and calculated patterns) is given by the blue curve at the bottom of the fit. The green vertical upper tick marks reflect the Bragg positions for nuclear reflections, and the lower green ticks give the Bragg positions for magnetic reflections.

Co and Zn. The average of 10 readings from this sample using SEM-EDS is $Co_{10.0(4)}Zn_{10.0(4)}$, which agrees well with the NPD refinement, and is consistent with the results of single-crystal X-ray diffraction on crystalline specimens extracted from a similarly loaded sample. As expected, the unit cell constant and isotropic displacement parameters for the 8c and 12d sites are larger at 500 K than those at 293 K. NPD refinement also indicated that polycrystalline β-Mn-type $Co_{10.0(4)}Zn_{10.0(4)}$ showed some preferred orientation along the {001} family of directions.

As part of a brief discussion of the structural chemistry of the α-Mn and β-Mn structures, Nesper suggested that the majority (12d) site in β-Mn might have slightly cationic character and the minority (8c) site has slightly anionic character.[42,53] Evaluation of the charge densities at the 8c and 12d sites using Bader analysis for various β-Mn model structures with late 3d metal atoms (Co−Zn) supports Nesper's suggestion (see Table S4 in the Supporting Information) by yielding the 8c sites as valence electron-*rich* and the 12d sites as valence electron-*poor*. Nonetheless, a qualitative assessment of the site preferences using atomic electronegativities remains unclear for the Co−Zn system. In particular, depending upon the electronegativity scale, there is no clear differentiation between Co and Zn. According to Pauling's scale, which used bond enthalpies to estimate the electronegativities,[54] and Allen's configuration energies,[55] Co (1.88 and 10.85 eV) is more electronegative than Zn (1.65 and 9.39 eV). On the other hand, Mulliken's scale or Pearson's absolute electronegativities,[56] which are derived from gas-phase ionization energies and

Table 5. Refined Parameters of an Equimolar β-Mn-Type Co−Zn Phase As Determined by Rietveld Refinement of NPD Data at 293 and 500 K[a]

atom	Wyckoff site	occupancy	x	y	z	U (Å^2)
293 K [a = 6.3343(1) Å]; R_p = 3.83; R_{wp} = 5.17; R_{exp} = 3.16; Bragg R factor = 4.41; χ^2 for fit = 2.69						
Zn/Co	12d	0.80(2)/0.20	$^1/_8$	0.2033(1)	0.4532(1)	0.61(3)
Co2	8c	1	0.0648(1)	0.0648(1)	0.0648(1)	0.63(3)
ferromagnetic moment = 0.85(3) μ_B/Co						
500 K [a = 6.3547(2) Å]; R_p = 8.00; R_{wp} = 11.0; R_{exp} = 4.88; Bragg R factor = 7.68; χ^2 for fit = 1.86						
Zn/Co	12d	0.80(2)/0.20	$^1/_8$	0.2028(2)	0.4533(5)	0.94(4)
Co2	8c	1	0.0662(5)	0.0662(5)	0.0662(5)	0.98(4)

[a]Numbers in parentheses are standard uncertainties in the last given digit from Rietveld fits.

dx.doi.org/10.1021/ic4009653 | *Inorg. Chem.* 2013, 52, 9399−9408

Table 6. Relative Total Energies (ΔE; meV/unit cell) with Respect to the Lowest-Energy Model for Various Atomic Distributions in β-Mn-Type $Co_{10}Zn_{10}$

		model				
		I	II	III	IV	V
formulation	8c	Co_8	Co_6Zn_2	Co_4Zn_4	Co_2Zn_6	Zn_8
	12d	Co_2Zn_{10}	Co_4Zn_8	Co_6Zn_6	Co_8Zn_4	$Co_{10}Zn_2$
ΔE (meV/fu)		0(4)	111(4)	195(12)	264(30)	264(4)
μ (μ_B/fu)		12.8−13.0	11.8−12.4	12.4−13.3	13.9−14.1	∼14.2

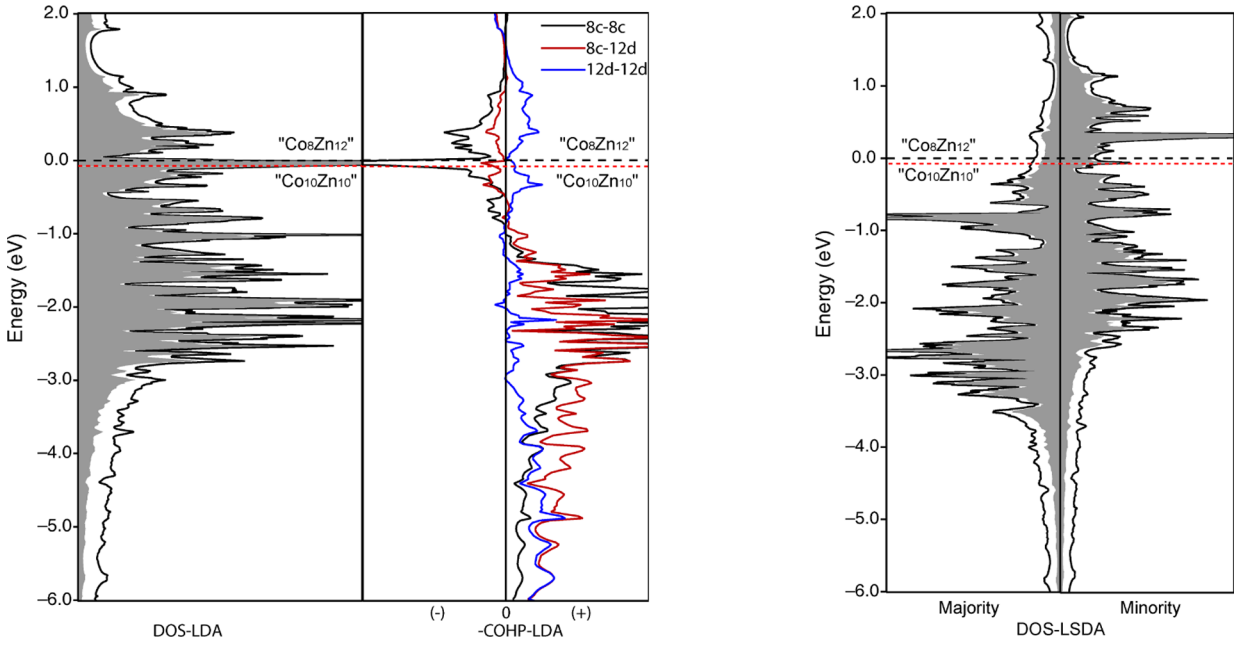

Figure 4. (Left) Partial DOS curves and −COHP curves of "Co_8Zn_{12}" obtained from nonspin polarization (LDA; + is bonding/− is antibonding). (Right) Partial DOS curves of "Co_8Zn_{12}" obtained from spin polarization (LSDA). E_F for 216e$^-$ is set to zero.

electron affinities, indicate the opposite, with Zn (4.45 eV) more electronegative than Co (4.27 eV). Nevertheless, in such an intermetallic compound, metallic properties would preclude any significant charge transfer between atoms but do not discount a redistribution of orbital occupations from the ground-state gaseous atoms. In fact, relative atomic sizes as reflected in 12-coordinate metallic radii may be more discriminating for observed β-Mn-type examples. The 8c site, which is fully occupied by Co (1.25 Å) in $Co_{8+x}Zn_{12-x}$, Ru (1.34 Å) in Mg_3Ru_2, and Fe (1.26 Å) in Re_3Fe_2, attracts the smaller atom, whereas Zn (1.37 Å), Mg (1.60 Å), and Re (1.37 Å) fill the majority 12d sites. Only in Mg_3Ru_2 does the electronegativity argument parallel the size argument. Therefore, quantum-chemical calculations are warranted to examine possible driving forces arising from the electronic structure that influence the structural stability and site preferences in β-Mn-type $Co_{8+x}Zn_{12-x}$.

Electronic Structure and Chemical Bonding. To examine possible electronic influences for the site preferences in $Co_{8+x}Zn_{12-x}$, VASP calculations were employed to evaluate the total energies and magnetic moments of five different cases (**I**−**V**) of β-Mn-type $Co_{10}Zn_{10}$ (x = 2) with various elemental distributions on the 8c and 12d sites. For each case, four distinct arrangements were calculated. The average relative total energies, their corresponding standard deviations, and the ranges of magnetic moments per formula unit are listed for each case in Table 6 (specific results are summarized in Table S5 in the Supporting Information). Among these five cases, expressed as $(8c)_8(12d)_{12}$, **I** most closely resembles the experimental results with Co atoms filling the 8c sites and **III** is closest to a statistical occupation of both crystallographic sites. According to the relative total energies in Table 6, the experimental result with Co fully occupying the 8c sites clearly gives the overall lowest energy. A linear regression analysis using the total energies of models **I**−**IV** estimates a rise in the total energy by ∼44(2) meV/Zn atom in the 8c site. Fluctuations in the tabulated energies originate from the specific atomic locations within each model. Somewhat surprising, however, are the comparable total energies between models **IV** and **V**, a result that arises from similar coordination environments in these structural models.

To gain further insight into the electronic influences on the site preference problem and phase width, as well as possible magnetic properties of the β-Mn-type $Co_{8+x}Zn_{12-x}$, TB-LMTO-ASA calculations were carried out to evaluate and analyze the electronic DOS. With the LDA, the corresponding DOS curve for a hypothetical "Co_8Zn_{12}" (216 valence electrons) is illustrated in Figure 4, which emphasizes contributions from the Co valence orbitals (a more detailed orbital decomposition of the DOS curve is shown in Figure S4 in the Supporting Information). Most of the DOS curve between −3 and +1 eV (0 eV = Fermi level for 216 valence electrons) belongs to the Co 3d band; below −3 eV is a ∼5 eV tail comprising a combination of Co and Zn 4s orbital contributions. The Zn 3d orbitals create a narrow band located ∼7−8 eV below the Fermi level. In the LDA-DOS curve, the Co 3d band exhibits

dx.doi.org/10.1021/ic4009653 | Inorg. Chem. 2013, 52, 9399−9408

little fine structure except for a noticeable pseudogap at approximately −0.5 eV (204 valence electrons) and a sharp, intense peak, which is ∼0.1 eV wide, just below 0 eV. According to the corresponding COHP curves, the wave functions contributing to this peak have strong 8c−8c(Co−Co) antibonding character. The pseudogap at −0.5 eV is associated with optimization of 8c−12d(Co−Zn) orbital interactions in this structure. On the other hand, the LDA band structure (shown in Figure S5 in the Supporting Information) reveals that the peak involves Co 3d bands that are relatively flat (nearly dispersionless) near the Brillouin zone boundaries (near point M and along the direction M−R). These features of the LDA-DOS arise from structural influences on the orbital interactions in β-Mn-type $Co_{8+x}Zn_{12-x}$. The Fermi level for $Co_{10}Zn_{10}$ (210 valence electrons) is located on the lower-energy edge of the peak just below 0.0 eV. Evaluation of the Stoner condition using the Co partial DOS gives $N(Co)I(Co) = 1.56$, where $N(Co) = 3.18$ eV^{-1} and $I(Co) = 0.49$ eV.[57,58] Thus, according to the LDA-DOS curves, β-Mn-type $Co_{8+x}Zn_{12-x}$ ($x \sim 2$) is susceptible either toward a possible structural distortion by disrupting the antibonding Co−Co orbital interactions at the Fermi level or toward ferromagnetism by breaking the spin degeneracy.[59] To a first approximation, the Stoner condition for ferromagnetism is satisfied.

Applying spin polarization via LSDA splits the DOS curves for the spin-up and spin-down wave functions, as seen in Figure 4. The corresponding Fermi levels for 210 and 216 valence electrons are shifted away from the peaks in the DOS curves and closely approach the pseudogap in the minority spin DOS curve, at which the 8c−12d(Co−Zn) orbital interactions in this manifold of wave functions are optimized and occupation of 8c−8c antibonding states is avoided (see Figure S6 in the Supporting Information). Therefore, the contribution from 8c−8c(Co−Co) orbital interactions constitute ca. 20.5% of the summed integrated COHP values over all interatomic contacts of less than 4.2 Å in $Co_{10}Zn_{10}$. The 8c−12d metal−metal interactions contribute ca. 46% (see Table S6 in the Supporting Information). The DOS also show peaks located at ca. −0.85 and +0.3 eV, respectively, in the majority and minority spin curves, features that arise from similar band dispersions seen in the LDA-DOS and LDA band structures (see also Figure S5 in the Supporting Information). Integration of the spin-up and spin-down DOS curves yields a total magnetic moment of 11.9 μ_B per formula unit for $Co_{10}Zn_{10}$. Analysis of the local moments reveals essentially no net unpaired spins at each Zn atom, so the result corresponds to 1.19 μ_B per Co atom. Furthermore, the majority spin Co 3d band is not completely filled at the Fermi level, so the result also indicates soft ferromagnetic behavior.

Magnetization Measurements. The isothermal magnetization curves of β-Mn-type $Co_{10.0(2)}Zn_{10.0}$ [loaded as 49.85(1) atom % Zn] measured at 2 and 300 K indicate the sample to be ferromagnetic. Table 7 summarizes the results of this magnetization study. Saturation is achieved at 10.0 kOe at 2 K. The saturation moments are obtained from hysteresis 13.0(2) μ_B/fu at 2 K and 10.3(2) μ_B/fu at 300 K.[60] The saturation moment observed at 2 K agrees well with the value of the total magnetic moment per unit cell (formula unit) calculated by electronic structure methods. Moreover, temperature-dependent magnetic susceptibility measurements from 300 to 600 K confirm the ferromagnetic nature of the phase $Co_{10.0(2)}Zn_{10.0}$ with a Curie temperature of 418(15) K (see Table 7 and Figure 5).

Table 7. Magnetic Data of $Co_{10.0(1)}Zn_{10.0}$ from Magnetization Measurements, NPD, and Theoretical Calculations

	μ_{SAT} at 2 K (μ_B/fu)	μ_{SAT} at 300 K (μ_B/fu)	μ_{EFF} (μ_B/fu)	μ(Co) (μ_B)	T_{Curie} (K)
SQUID, VSM	13.0(2)	10.3(2)	8.5(2)		418(15)
NPD				0.85(3)	∼420
theory	11.9				

From NPD, the magnetic structure of as-loaded $Co_{10.0(1)}Zn_{10.0}$ was refined in the space group $P\bar{1}$, with a refined composition $Co_{10.4(2)}Zn_{9.6}$. Modeling of the magnetic intensities at 293 K revealed a ferromagnetic structure, giving a local Co moment of 0.85(3) μ_B with the direction at each Co atom pointing along the crystallographic c direction, and a total effective moment of 8.8(4) μ_B. This value agrees well with an effective moment of 8.5(2) μ_B obtained from a linear Curie−Weiss fit of the magnetic susceptibility data evaluated between 450 and 600 K. In addition, from the NPD magnetization measurement, the Curie point is around 420 K, which is consistent with the magnetic measurement by VSM.

Taking the magnetization study and calculated electronic structure into account, the magnetic behavior of β-Mn-type $Co_{8+x}Zn_{12-x}$ ($x \sim 2$) is best described by local moments located at the Co atoms interacting via electrons in the conduction band. The absence of temperature-independent Pauli paramagnetism above the Curie point of ∼420 K and the presence of both Curie−Weiss (linear) high-temperature behavior and the split flat-band regions on the Brillouin zone boundaries in the electronic band structure point toward this local moment behavior, even though the Stoner condition is well met by the LDA-DOS curve for $Co_{8+x}Zn_{12-x}$ ($x \sim 2$). To gain a better understanding of the structure−magnetic relationships in these Co−Zn and related β-Mn-type systems, semiempirical DFT +U[61] methods will be employed to examine how the orbital overlaps and electron−electron interactions affect the band structure and electronic distributions in these systems.

CONCLUSIONS

β-Mn-type $Co_{8+x}Zn_{12-x}$ [1.7(2) < x < 2.2(2)] phases were synthesized and structurally characterized. They exhibit a small homogeneity width, with Co atoms exclusively occupying the 8c sites in the noncentrosymmetric cubic structure. Moreover, the magnetic properties of a sample analyzed as $Co_{10.0(2)}Zn_{10.0}$, i.e., equiatomic in Co and Zn, show it to be a high-temperature, ferromagnetic material with a Curie point of ∼420 K. First-principles electronic structure calculations substantiate the ferromagnetic ground state and indicate that the saturation magnetization is derived essentially from local moments at the Co sites interacting via the conduction electrons. The binary β-Mn-type structure of $Co_{8+x}Zn_{12-x}$ can be derived from the cubic Laves phase structure, $MgCu_2$ type, by creating ordered vacancies in the majority atom (Cu) positions. The arrangement of these vacancies is driven primarily by minimizing the electrostatic energy between the conduction electrons and the positive nuclei. This structural analysis demonstrates a significant relationship between β-Mn-type structures and diamond-like lattices and is providing greater insight into the complex structures of both α-Mn- and β-Mn-type structures.[53]

dx.doi.org/10.1021/ic4009653 | Inorg. Chem. 2013, 52, 9399−9408

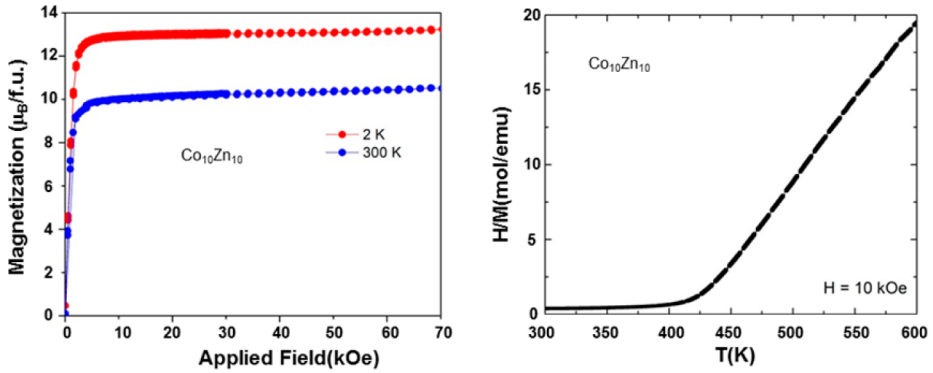

Figure 5. (Left) Hysteresis curves at 2 K and 300 K and (right) $\chi_m^{-1}(T)$ curve measured in 10 kOe field for β-Mn type $Co_{10(2)}Zn_{10}$. The corresponding magnetization vs temperature curve in 10 kOe field is shown in Figure S7 in Supporting Information.

■ ASSOCIATED CONTENT

Supporting Information

Tables of anisotropic temperature factors and significant interatomic distances of β-Mn-type $Co_{8+x}Zn_{12-x}$ single crystals, a distance comparison among various β-Mn-type structures, results of a Bader charge analysis, specific energies and magnetic moments from $Co_{10}Zn_{10}$ models, integrated COHP values of $Co_{10}Zn_{10}$, as well as figures of powder X-ray diffraction, electron micrographs, structures of nine defect cubic Laves phases, partial DOS curves and band structures for "Co_8Zn_{12}", and a magnetization versus temperature curve for $Co_{10.0(2)}Zn_{10.0}$. This material is available free of charge via the Internet at http://pubs.acs.org.

■ AUTHOR INFORMATION

Corresponding Author

*E-mail: gmiller@iastate.edu.

Notes

The authors declare no competing financial interest.

■ ACKNOWLEDGMENTS

This work was carried out at the Ames Laboratory, which is operated for the U.S. Department of Energy by Iowa State University under Contract DE-AC02-07CH11358. This work was supported by the U.S. Department of Energy, Office of Basic Energy Sciences, Division of Materials Sciences and Engineering. The authors thank Dr. Wei Tang in the Ames Laboratory for magnetic measurements, Dr. Warren E. Straszheim in the Ames Laboratory for SEM analysis, and three astute reviewers for their insightful comments and suggestions.

■ REFERENCES

(1) Hume-Rothery, W. *J. Inst. Met.* **1926**, *35*, 295.
(2) Mizutani, U., *Hume-Rothery Rules for Structurally Complex Alloy Phases*; CRC Press: New York, 2011.
(3) Asahi, R.; Sato, H.; Takeuchi, T.; Mizutani, U. *Phys. Rev. B* **2005**, *B72*, 125102.
(4) Gourdon, O.; Miller, G. J. *J. Solid State Chem.* **2003**, *173*, 137.
(5) Gourdon, O.; Bud'ko, S. L.; Williams, D.; Miller, G. J. *Inorg. Chem.* **2004**, *43*, 3210.
(6) Ko, H.; Gourdon, O.; Gout, D.; Mun, E.-D.; Thimmaiah, S.; Miller, G. J. *Inorg. Chem.* **2010**, *49*, 11505.
(7) Vassilev, G. P.; Jiang, M. *J. Phase Equilib. Diffus.* **2004**, *25*, 259.
(8) Takayama, T.; Shinohara, S.; Ishida, K.; Nishizawa, T. *J. Phase Equilib.* **1995**, *16*, 390.
(9) Okamoto, H. *J. Phase Equilib.* **2003**, *24*, 280.
(10) Buschow, K. H. J.; Van Engen, P. G.; Jongebreur, R. *J. Magn. Magn. Mater.* **1983**, *38*, 1.
(11) Boström, M.; Lidin, S. *J. Solid State Chem.* **2002**, *166*, 53.
(12) Lind, H.; Boström, M.; Petricek, V.; Lidin, S. *Acta Crystallogr., Sect. B* **2003**, *59*, 720.
(13) Skyrme, T. *Nucl. Phys.* **1962**, *31*, 556.
(14) Mühlbauer, S.; Binz, B.; Jonietz, F.; Pfleiderer, C.; Rosch, A.; Neubauer, A.; Georgii, R.; Böni, P. *Science* **2009**, *323*, 915.
(15) Yu, X. Z.; Kanazawa, N.; Onose, Y.; Kimoto, K.; Zhang, W. Z.; Ishiwata, S.; Matsui, Y.; Tokura, Y. *Nat. Mater.* **2011**, *10*, 106.
(16) Hama, T.; Matsumura, M.; Kato, H.; Yamagataa, H.; Kohori, Y.; Kohara, T.; Iwamoto, Y. *J. Phys. Soc. Jpn.* **2004**, *73*, 2305.
(17) Elenius, M.; Zetterling, F. H. M.; Dzugutov, M.; Fredrickson, D. C.; Lidin, S. *Phys. Rev. B* **2009**, *79*, 144201.
(18) Lidin, S.; Fredrickson, D. *Symmetry* **2012**, *4*, 537.
(19) Wang, N.; Chen, H.; Kuo, K. H. *Phys. Rev. Lett.* **1987**, *59*, 1010.
(20) Wang, N.; Fung, K. K.; Kuo, K. H. *Appl. Phys. Lett.* **1988**, *52*, 2120.
(21) *PowderCell*, version 2.3; Federal Institute for Materials Research and Testing: Unter den Eichen, Berlin, Germany, 2000.
(22) Rietveld, H. M. *J. Appl. Crystallogr.* **1969**, *2*, 65.
(23) Hunter, B. A.; Howard, C. J. *LHPM-Rietica*, version 1.71; Australian Nuclear Science and Technology Organization: Menai, Australia, 2000.
(24) Sheldrick, G. M. *SADABS*; University of Gottingen: Gottingen, Germany, 2001.
(25) Sheldrick, G. M. *Acta Crystallogr., Sect. A* **2008**, *64*, 112.
(26) *SHELXTL*, version 6.10; Bruker AXS Inc.: Madison, WI, 2000.
(27) *Diamond*, version 3.2; Crystal Impact: Bonn, Germany, 2010.
(28) Rodriguez Caravajal, J. *FULLPROF*, version 3.2; Laboratoire Léon Brillouin: Saclay, France, 1997.
(29) Jepsen, O.; Andersen, O. K. *TB-LMTO*, version 47; Max-Planck-Institut für Festkörperforschung: Stuttgart, Germany, 2000.
(30) von Barth, U.; Hedin, L. *J. Phys. C: Solid State Phys.* **1972**, *5*, 1629.
(31) Lambrecht, W. R. L.; Andersen, O. K. *Phys. Rev. B* **1986**, *34*, 2439.
(32) Kresse, G.; Hafner, J. *Phys. Rev. B* **1993**, *47*, 558.
(33) Kresse, G.; Hafner, J. *Phys. Rev. B* **1994**, *49*, 14251.
(34) Kresse, G.; Furthmüller, J. *Comput. Mater. Sci.* **1996**, *6*, 15.
(35) Kresse, G.; Furthmüller, J. *Phys. Rev. B* **1996**, *54*, 11169.
(36) Tang, W.; Sanville, E.; Henkelman, G. *J. Phys.: Comput. Mater.* **2009**, *21*, 084204.
(37) Sanville, E.; Kenny, S. D.; Smith, R.; Henkelman, G. *J. Comput. Chem.* **2007**, *28*, 899.
(38) Henkelman, G.; Arnaldsson, A.; Jónsson, H. *Comput. Mater. Sci.* **2006**, *36*, 254.
(39) Monkhorst, H. J.; Pack, J. D. *Phys. Rev. B* **1976**, *13*, 5188.
(40) Blöchl, P. E.; Jepsen, O.; Andersen, O. K. *Phys. Rev. B* **1994**, *49*, 16223.

(41) Massalski, T. B.; Okamoto, H. *Binary Alloy Phase Diagrams*; ASM International: Novelty, OH, 1990.
(42) Nesper, R. *Prog. Solid State Chem.* **1990**, *20*, 1.
(43) Errandonea, D.; Ferrer-Roca, C.; Martinez-Garcia, D.; Segura, A.; Gomis, O.; Munoz, A.; Rodriguez-Hernandez, P.; Lopez-Solano, J.; Alconchel, S.; Sapina, F. *Phys. Rev. B* **2010**, *82*, 174105.
(44) Burdett, J. K.; McLarnan, T. J. *Inorg. Chem.* **1982**, *21*, 1119.
(45) Jeitschko, W.; Nowotny, H. N.; Benesovsky, F. *Monatsh. Chem.* **1963**, *94*, 247.
(46) Wang, F.; Miller, G. J. *Inorg. Chem.* **2011**, *50*, 7625.
(47) Pauling, L. *Proc. Natl. Acad. Sci. U. S. A.* **1987**, *84*, 3537.
(48) Urban, K.; Feuerbacher, M. *J. Non-Cryst. Solids* **2004**, *334&335*, 143.
(49) Ohba, T.; Kitano, Y.; Komura, Y. *Acta Crystallogr.* **1984**, *40*, 1.
(50) Pottgen, R.; Hlukhyy, V.; Baranov, A.; Grin, Y. *Inorg. Chem.* **2008**, *47*, 6051.
(51) Kuz'ma, Y. B.; Kripyakevich, P. I. *Kristallografiya* **1965**, *10*, 558.
(52) Morozkin, A. V. *Intermetallics* **2012**, *25*, 136.
(53) Nesper, R. *Angew. Chem., Int. Ed. Engl.* **1991**, *30*, 789.
(54) Pauling, L. *J. Am. Chem. Soc.* **1932**, *54*, 3570.
(55) Allen, L. C. *J. Phys. Chem.* **1993**, *97*, 5787.
(56) Mulliken, R. S. *J. Chem. Phys.* **1934**, *2*, 782.
(57) Seo, D. K.; Kim, S. H. *J. Comput. Chem.* **2008**, *29*, 2172.
(58) Janak, J. F. *Phys. Rev. B* **1977**, *16*, 225.
(59) Dronskowski, R. *Computational chemistry of solid state materials*; Wiley-VCH: New York, 2008.
(60) Jiles, D. *Introduction to magnetism and magnetic materials*; Chapman & Hall: New York, 1998.
(61) Liechtenstein, A. I.; Anisimov, V. I.; Zaanen, J. *Phys. Rev. B* **1995**, *52*, 5467.